Elsevier Editorial System(tm) for Electrochimica Acta

Manuscript Draft

Manuscript Number: PK15-384R1

Title: Growth of polypyrrole nanostructures through reactive templates for energy storage applications

Article Type: Research Paper

Keywords: Polypyrrole, Nanostructures, Supercapacitors, Li-ion battery

Corresponding Author: Dr. Deepak Dubal, M.Sc.Ph.D.

Corresponding Author's Institution: Catalan Institute of Nanoescience and Nanotechnology

First Author: Deepak Dubal, M.Sc.Ph.D.

Order of Authors: Deepak Dubal, M.Sc.Ph.D.; Zahilia Caban-Huertas; Rudolf Holze; Pedro Gomez-Romero

Abstract: This work presents a facile reactive template route to prepare polypyrrole (PPy) with a given, chosen nanostructure among three different morphologies (i.e., nanotubes, nanofibers and urchins). This approach exploits the variability of MnO2 morphologies and its versatility as sacrificial template. The morphological evolution for this template-assisted growth of PPy nanostructures has been briefly explained. These unique architectures significantly enhance the electroactive surface area of the PPy nanostructures, leading to better interfacial/chemical distribution at the nanoscale, fast ion and electron transfer and good strain accommodation. Thus, when used as supercapacitor electrodes, a maximum specific capacitance of 604 F/g at a current density of 1.81 A/g was reached for PPy nanofibers. Even after more than 1000 cycles at 9 A/g, a capacitance of 259 F/g with 91 % retention was achieved. Moreover, the same PPy nanofibers can be used as cathode material for lithium-ion batteries (LIBs), showing a capacity of 70.82 mAh/g at a rate of 0.10 C with good cycling stability and rate capability. Our results provide sound evidences that PPy nanostructures can be properly tuned and make the difference for the practical application of these materials in electrochemical energy storage devices.

Growth of polypyrrole nanostructures through reactive templates for energy storage applications

Deepak P. Dubal[a,b]*, *Zahilia Caban-Huertas*[a], *Rudolf Holze*[b], *Pedro Gomez-Romero*[a]*

[a]Catalan Institute of Nanoscience and Nanotechnology, CIN2, ICN2 (CSIC-ICN), Campus UAB, E-08193 Bellaterra, Barcelona, Spain

[b]Technische Universität Chemnitz, Institut für Chemie, AG Elektrochemie, D-09107 Chemnitz, Germany

CORRESPONDING AUTHOR FOOTNOTE

Dr. Deepak Dubal, and Prof. Pedro Gomez-Romero

Tel.: +349373609/+345929950 Fax: +345929951

E-mail: dubaldeepak2@gmail.com (D. Dubal),

pedro.gomez@cin2.es (P. Gomez-Romero)

Abstract

This work presents a facile reactive template route to prepare polypyrrole (PPy) with a given, chosen nanostructure among three different morphologies (i.e., nanotubes, nanofibers and urchins). This approach exploits the variability of MnO_2 morphologies and its versatility as sacrificial template. The morphological evolution for this template-assisted growth of PPy nanostructures has been briefly explained. These unique architectures significantly enhance the electroactive surface area of the PPy nanostructures, leading to better interfacial/chemical distribution at the nanoscale, fast ion and electron transfer and good strain accommodation. Thus, when used as supercapacitor electrodes, a maximum specific capacitance of 604 F/g at a current density of 1.81 A/g was reached for PPy nanofibers. Even after more than 1000 cycles at 9 A/g, a capacitance of 259 F/g with 91 % retention was achieved. Moreover, the same PPy nanofibers can be used as cathode material for lithium-ion batteries (LIBs), showing a capacity of 70.82 mAh/g at a rate of 0.10 C with good cycling stability and rate capability. Our results provide sound evidences that PPy nanostructures can be properly tuned and make the difference for the practical application of these materials in electrochemical energy storage devices.

Introduction

Increasing global demand of energy and the emergence of intermittent renewables is putting energy storage in the spotlight. Improved yet low-cost electrochemical energy storage devices with high performance electrode materials are thus in growing demand. [1-3] Among energy storage systems, supercapacitors along with lithium ion batteries (LIBs) have demonstrated its versatility and are in the process of expanding to different niche applications thanks to their inherent electrochemical properties as well as cost effectiveness. [4-6] Supercapacitors, as the new family member of electrochemical energy storage systems have drawn considerable attention due to their fast charge-discharge characteristics, high power density, and excellent cycle stability. [7-9] Commonly, there are two different charge storing mechanisms observed in supercapacitors: i) non-faradaic, in which ions are adsorbed at the electrode surface upon polarization and ii) pseudocapacitive, which is of faradaic nature, in which charges are stored through surface redox reactions. Ultimately, supercapacitor performance is largely determined by the surface properties of a given electrode material, properties such as electrochemically active surface area, nanostructure, porosity and so forth.

On the other hand, Li-ion batteries are designed so that they can provide high energy density by storing charge in bulk electrodes (bulk storage) through faradaic reactions. [10-12] In the case of Li-ion batteries, large efforts are devoted to investigate different kinds of electrode active materials which can provide high energy density, high capacity, good cycling stability and suitable efficiency for lithiation/de-lithiation. [13-15]

Conducting polymers have long waved a flag of promise as electroactive storage materials based on their reversible redox properties, low cost, light weight and polymeric nature that led to dream of plastic batteries since their discovery. Indeed, conducting polymers could be

considered a unique flagship among electroactive materials due to their unique π-conjugated structure and switchable conductivity between insulator and metal. [16, 17] But, as it was hinted above, their final performance is not so much dependent upon their intrinsic properties as on their microstructure. That is why most of the recent research efforts in the field are devoted to the nanostructuration of conducting polymers which ultimately affects their physical-chemical properties and allows *ad-hoc* designs for various applications such as molecular electronics, optics, catalysis and energy storage. [18-20]

Polypyrrole (PPy) is one of the most thriving members of the conducting polymers family owing to its inherent properties such as excellent conductivity, redox properties, environmental stability, biocompatibility and so forth.[21.-23] Nevertheless, it is still surprisingly challenging to fabricate any desired nanostructure of polypyrrole (PPy). Most common approaches for the fabrication of diverse nanostructures of PPy include hard and soft templating methods. However each of these categories has its own drawbacks. The hard template approach needs additional template removal treatments which can damage the original nanostructure whereas soft template methods involve the use of doping polyanions, surfactants etc. which raise environmental concerns. [24-26] To the best of our knowledge, there are very few reports about the fabrication of PPy hierarchical structures constructed from nanostructured building blocks using reactive templates.[27, 28]

Here we provide a systematic approach towards the control of conducting polymer microstructures through the use of pre-formed metal oxide nanostructures which can be used as templates to create novel nanostructures for conducting polymers. Three different morphologies of PPy (i.e., nanotubes, nanofibers and urchins) were prepared by exploiting the crystallographic versatility of MnO_2 through the corresponding nanostructures of this oxide (i.e. nanorods,

nanowires, urchins) as sacrificial templates. These unique architectures significantly enhance the electroactive surface areas of the PPy nanostructures, leading to excellent electrochemical properties when used as LIB or as supercapacitor electrode materials. Furthermore, the electrochemical properties of nanostructured PPy electrodes were systematically investigated. Their performance is highly dependent on the morphology of the PPy, highlighting the importance of the morphology-controlled process reported here.

Results and discussion

Fig. 1 (a-c) shows three different morphologies of MnO_2, namely, nanorods, nanowires and urchins, which were used as sacrificial templates to prepare nanotubes, nanofibers and urchins of PPy, respectively (see Fig. 1 (d-f)). It is interesting to note that even after a dense deposition of PPy, all three original nanostructures of MnO_2 were successfully retained by the polymer. The formation mechanism of PPy nanostructures can be rationalized as follows and it is schematically shown in Fig. 2. Initially, pyrrole monomers are adsorbed on the outer surface of solid MnO_2 nanostructures yielding an adsorbate-covered solid-liquid interface. Then the redox reaction between MnO_2 and pyrrole monomers takes place at the interface in the presence of HCl, which results in the formation of oligo- and polymeric species (PPy) of pyrrole following an instantaneous dissolution of MnO_2. The interfacial polymerization of PPy continues until the complete removal of MnO_2 and the nanostructured PPy is finally obtained. The oxidation potential of MnO_2 ($E_{MnO_2/Mn^{2+}}$) is 1.23 V [29, 30], which is high enough for the polymerization of pyrrole monomers on the surface of MnO_2 since the oxidation potential of pyrrole monomers is about 0.7 V.[27, 28] As the redox reactions proceed, the rigid templates are sacrificed while the pyrrole monomers are polymerized surrounding the templates, which leads to the formation of

the aforementioned PPy nanostructures. From Fig. 1 (d-f), it is revealed that PPy nanostructures are found to have a larger outer diameter than that of MnO_2 nanostructures, suggesting favorable outward growth of PPy through a diffusion-controlled process. On the other hand, the larger diameter of PPy nanostructures can be ascribed to the volume-expansion during the conversion of PPy from MnO_2 since the density of PPy is much lower than that of MnO_2. Thus, using nanorods and nanowires of MnO_2, we have prepared 1D PPy nanotubes and nanofibers whereas 3D urchin-shape PPy is formed from the straight and radially arranged PPy nanotubes. These hierarchical PPy structures are totally inherited from the MnO_2 templates, indicating the reactive template synthesis is effective to prepare PPy complex architectures through an eco-friendly one-step technique.

Fig. 3 shows TEM images of the three different PPy nanostructures. Fig. 3 (a, b) shows TEM images of the resulting 1D PPy nanostructures: nanotubes and nanofibers, respectively. It is confirmed that the PPy nanostructures replicate the 1D shape of MnO_2 templates. TEM image shows the nanotubular structure with a smooth inside and uneven outside as well as a uniform tube wall thickness for PPy nanotubes (see Fig. 3 (a)). In the case of nanofibers, clustered hollow and long fibers are observed (Fig. 3 (b)). It is worth pointing out that PPy layers grow on the surface of the MnO_2 templates, resulting in larger outer diameters. On the other hand, Fig. 3 (c) shows 3D PPy urchins with a diameter of about 3-4 μm. These urchins are characterized by a porous surface with multiple straight and radially arranged PPy nanotubes. The diffuse ring of the selected area electron diffraction pattern (SAED, Fig. 3(d)) indicates the amorphous structure of PPy urchins.

XRD for all three PPy nanostructures are shown in Fig. 4 (a). For all three PPy samples, characteristic peaks of PPy are centered at around 24.6°, which correspond to the repeating unit

of the pyrrole ring, implying the polymer chain is highly oriented. [31] On the other hand, the very broad peaks reveal a small crystallite size far from any long-range crystalline order. Moreover, the intensity of the peaks for PPy nanotubes and urchins is relatively higher than that of PPy nanofibers, suggesting the appearance of a relatively more ordered structure and the decrease of the polymer chain distance. This is due to the ordered pore structure in PPy nanofibers as shown in their SEM and TEM images. Fig. 4 (b) shows full XPS survey scan spectra of PPy nanostructures. It is seen that all three PPy samples show the presence of oxygen (O 1s at ~532 eV), nitrogen (N 1s at ~399.8 eV), carbon (C 1s at ~284.5 eV) and chlorine (Cl 2p at ~199.5 eV), corresponding to the typical spectra of HCl-doped PPy, which is in good agreement with the reported ones. [32, 33] The elements carbon and nitrogen are from the polypyrrole backbone whereas the element chlorine is from the hydrochloric acid used in the polymerization process. [34] The element oxygen has probably originated from the surface oxidation of polypyrrole, or weakly charge-transfer-complexed oxygen atoms. [33]

N_2 adsorption-desorption measurements were used to study the porosity and textural properties of PPy nanostructures. The adsorption-desorption isotherms of PPy nanostructures are depicted in Fig. 5 (a). The isotherm can be labeled as type IV according to the IUPAC classification. Notably, a distinct hysteresis loop can be observed in the larger range of ca. 0.6–1.0 P/P_0, suggesting that the PPy nanostructures have a typical mesoporous structure, which is further supported by the Barrett-Joyner-Halenda (BJH) pore size distribution (PSD) data shown in Fig. 5 (b). As seen in Fig. 5 (a), the BET surface areas of PPy nanofibers (52.2 m^2/g) and PPy urchins (60.1 m^2/g) are relatively higher than that of PPy nanotubes (42.1 m^2/g), highlighting the much increased surface areas of PPy nanostructures which is attributed to their porous nature. These values are as high and/or comparable to other reported values for PPy nanostructures. [35,

[36] For example, in one of our previous reports, PPy nanostructures were synthesized by electrochemical polymerization method and surface areas ranging from 22.6 to 37.1 m^2/g were obtained.[37] Shinde et al. synthesized PPy nanoparticles with surface area of 55 m^2/g. [38] The average pore sizes of PPy nanostructures are found to be in the range of 10-12 nm with different pore volumes such as 0.12, 0.15, 0.16 cm^3/g for PPy-NTs, PPy-NFs and PPy-Ur, respectively. Pore sizes are all much larger than the size of the electrolyte ions used in the energy storage devices and will allow fast flow of the electrolyte ions into the PPy electrode materials.

Electrochemical evaluation of supercapacitors

Fig. 6 shows the CVs and the corresponding charge/discharge (CD) curves of the three different nanostructures of PPy in 1 M H_2SO_4 electrolyte. As seen in Fig. 6 (a-c) CV curves for all three PPy sample (PPy-NTs, PPy-Ur and PPy-NFs) deviate from ideal rectangular shapes, confirming involvement of pseudocapacitive charge storing mechanism. This is also confirmed by the CD curves for all PPy samples which are not ideally linear (Fig. 6 (d-f)). A linear relation between the current density and different scan rates is observed, showing that the redox reaction is a diffusion-controlled process. Since the redox reactions involve doping and de-doping of ions from the electrolyte in the electrode, at lower scan rate, this implies that the ions can diffuse almost entirely into all the pores of the electrode. Furthermore, it is interesting to note that, in the case of PPy-NFs sample, CV curves exhibit quasi-rectangular shapes (Fig. 6 (c)), making the corresponding CD curves also quasi-symmetrical (Fig. 6 (f)) as compared to the other PPy nanostructures (PPy-NTs and PPy-Ur). Moreover, PPy-NFs have relatively higher current densities than PPy-NTs and PPy-Ur nanostructures at the same scan rate, indicating a much larger specific capacitance of PPy-NFs. It is further interesting to note that, as the nanostructure

changed from nanotubes to nanofibers with intermediate step of urchins the shapes of CV curves deviates from ideal rectangular shape. The intensity of the redox peaks indicates the electrochemical response of the PPy to the electrolyte. Impressively, intensity of redox peaks for PPy-NFs sample is relatively higher than other PPy nanostructures suggesting excellent interaction of PPy-NFs with electrolyte. In addition, due to hollow and thin walls of nanofibers allows fast diffusion and large electrochemical sites. The integrated area under the CV curves increase in the following order: PPy-NTs < PPy-Ur < PPy-NFs (Fig. 6 (a-c)). Similar behavior is observed for the CD curves, where the charge and discharge time increase in the same order (Fig. 6 (d-f)). The values of specific capacitances derived from the charge/discharge curves with the current densities are presented in Fig. 7 (a). It is found that PPy-NFs exhibit higher specific capacitances than the other two nanostructures. The highest specific capacitance obtained at the lowest current density of 1.81 A/g is 604 F/g for the PPy-NFs, 318 F/g for PPy-Ur and 186 F/g for PPy-NTs (all capacitance values are normalized to mass of polypyrrole nanostructure coated on carbon cloth 1.1 mg/cm^2). Furthermore, areal capacitance was calculated by dividing capacitance by area of electrode whereas volumetric capacitance was calculated by multiplying specific capacitance to density of polypyrrole (1.48 g/cm^3) and are plotted in Fig. 7 (b, c), respectively. The highest areal and volumetric capacitances are found to be 846 mF/cm^2 and 894 F/cm^3 for PPy nanofibers at current density of 2.5 mA/cm^2, respectively. It is interesting to note that the specific capacitance obtained for PPy-NFs is very close to its theoretical value (620 F/g).[39] Strikingly, the significant enhancement of specific capacitance of PPy has been achieved by properly tuning the morphology of the electrode material. This finding confirms that the electrochemical performance of PPy is highly dependent on morphology, which in turn determines the electrode-electrolyte interphase. In addition, all three PPy nanostructures show

good rate capability as seen from Fig. 7 (b). It is very interesting to note that although PPy-Urs have higher surface area than PPy-NFs, their capacitance is lower. This must be due to the limited diffusion and transport of the electrolyte ions to the bulk of the big PPy urchin-like particles, especially into their condensed cores, preventing the full utilization of the inner surface of the PPy urchins. In contrast, the much increased surface area of PPy-NFs over PPy-NTs contributed largely to their energy storage capacity, as the hollow nanostructures provide more exposed surface for electrochemical reaction to take place. In other words, the structure tortuosity (a parameter used to bridge the pore structure and the permeability of the materials) of PPy nanostructures varies with their morphology, porosity, pore size, and its distribution, which may also have an effect on the electrochemical performance of the PPy supercapacitors. The relative high tortuosity of PPy-Ur makes the electrolyte ions difficult to diffuse to the whole particles, resulting in modest electrochemical response and capacitance values, while the lower structure tortuosity of PPy-NF and PPy-NT contributes to easier and faster access of electrolyte ions to the materials, giving better electrochemical response and higher capacitance values. Nevertheless, the specific capacitance values of our PPy electrodes are comparatively higher than previously reported ones. For instance, Wang et al. [40] reported a specific capacitance of 273 F/g for PPy nanotubes at 0.5 A/g. For comparison, 172-197 F/g for PPy nanotubes synthesized using methyl orange (MO)/$FeCl_3$ [41, 42], 305 F/g for PPy nanowires prepared using cetyltrimethylammonium bromide (CATB) [43] and 142 F/g for PPy particles [44] have been reported. Moreover, Fan et al. [45] prepared PPy thin films on Ti foil by electrodeposition method and reported specific capacitance of 480 F/g. Shi et al. [46] reported a specific capacitance of 380 F/g for nanostructured conductive polypyrrole hydrogels synthesized *via* an interfacial polymerization method. In addition, the values reported here higher than PPy-graphene

composite materials. For example, Oliveira et al. [47] prepared free standing PPy/graphene nanocomposite and reported specific capacitance of 277.8 F/g whereas Zhang et al. [48] reported a specific capacitance of 375 F/g for polypyrrole wrapped graphene hydrogels.

Long cycle life and high rate capability are important parameters for the practical applications of supercapacitors. Following the above cycles, the PPy electrodes were subjected to continuous charging and discharging for 1000 cycles at a high current density of 9 A/g, shown in Fig. 7 (d). All three PPy nanostructures showed a small decrease of their capacitance during the first ca. 50 cycles, then remained essentially constant up to at least 1000 cycles. The overall stability of PPy-NFs is higher (91 %) than that of the other two (i.e. 86 % for PPy-NTs and 89 % PPy-Ur), when tested under the same current density of 9 A/g. This added a further advantage to PPy-NFs and confirmed the morphology dependence of the electrochemical properties of PPy. The high capacitance, excellent cycling stability, and good rate capability can be attributed to the unique morphologies and structures of PPy nanostructures. In particular, the hierarchical porous architecture of PPy-NFs greatly increases the surface area, promoting the electrolyte to diffuse more easily into the inner region of the electrode, which results in a high utilization of the electroactive material. Additionally, the hierarchical array possesses a favorable morphological and phase stability, helping to alleviate the structure or phase damage caused by volume expansion and redox reactions during the cycling process.

Electrochemical evaluation of PPy nanostructures in lithium-ion batteries

Since PPy can be reversibly switched between oxidized and reduced state, it can be used as a lithium-storage host. It is well-known that the electrochemical reaction occurring at the PPy electrode is a doping-extraction process. In a Li/PPy cell with $LiPF_6$ as the electrolyte, the PPy

electrode releases electrons and gains PF_6^- in its structure to keep electro-neutrality during charging or doping process; while it gains electrons and releases PF_6^- during discharging or extraction process.

We tested the three nanostructured PPy samples as electrodes in front of Li anodes, The battery performance of the samples were tested at various C rates between 2.0 and 4.5 V vs. Li/Li^+, but first the cells were cycled at 1C for 20 cycles and finally back at 1C for 100 cycles (see Fig. 8 (a, b)). In addition, the capacity can be recovered when the C-rate is turned back to 1C after cycling at various C-rates. This is indicative of an excellent electrochemical reversibility. The capacity fading was 2% if we take into account the last 100 cycles and we compare them with the first 5^{th} cycles performed at 1C. To be precise, capacities changed from 4.5 to 4 mAh/g in the case of the PPy-NFs, 6 to 5 mAh/g in the case of PPy-Urs and from 5.5 to 5 mAh/g in the case of the PPy-NTs. Another interesting thing observed was that when the C-rate increased, the sample that showed more capacity was PPy-Ur while at low C-rates PPy-NFs shows higher capacity. The nano-sized morphology of the particles plays a significant role with the utilization of particles being enhanced by their larger surface area and shorter diffusion length for the lithium intercalation process. At high C-rate the urchins have more pores available that results in more area for the electrolyte diffusion in this structure, which can explain the better performance of this structure at high C-rates (Fig. 8 (c)).

Evolution of cell resistance ESR over cycling was studied by electrochemical impedance spectroscopy. The EIS was conducted after the cell was charged/discharged before and after charge/discharge cycles from 100 kHz to 0.010 Hz. As shown in Fig. 8 (d), an intercept in the high frequency region is observed which corresponds to the ohmic resistance. The depressed semicircle indicates that the charge transfer resistance R_{ct} and a straight line in the low frequency

region represents the Warburg impedance W. These results are in agreement with observations during the charge/discharge cycles. The PPy-NFs sample shows low resistance before and after charge/discharge cycling than that of other PPy nanostructures, indicating excellent of PPy-NFs. The results obtained here show an improvement over other polypyrrole based cathodes. Park et al. [49] reported capacity of 20 mAh/g at C-rate equivalent to 0.10 C for bare PPy material. They reported an increment in capacity when they covalently bound ferrocene to PPy. This material showed a capacity of 34 mAh/g for the 1st cycle at 0.10 C-rate. Qie et al. [50] showed that the oxidants play a role in the properties of PPy as cathode. Thus, PPy prepared with $FeCl_3$ showed a capacity of 98 mAh/g, however the capacity began to fall dramatically after just 35 cycles.

We have studied two different applications of PPy nanostructures such as supercapacitor and Li-ion battery. Although both are energy storage devices, they have different charge storing mechanism. In Li-ion batteries, the charges are stored in bulk of electrode materials through redox reactions (diffusion-controlled process) and hence exhibit high energy density but low power density. However, pseudo-capacitors (a type of supercapacitor different than EDLC) stores charge through reversible redox reactions at electrode/electrolyte interface and lead to EDLC-like electrochemical features but much greater charge storage. Moreover, pseudocapacitive materials hold the promise of achieving battery-level energy density combined with the cycle life and power density of EDLCs.[51] Interestingly, in present investigation, the shapes of CV and CD curves (see Fig. 7) doesn't show well-defined sharp redox peaks (like battery-type materials), suggesting pseudo-capacitive behavior (like EDLC type materials) of PPy nanostructures.[52] The charge storage mechanism is based on the fast and reversible doping/undoping of PPy and can be written as:

$$[PPy^{+}]SO_4^{2-} + 2e^{-} \Leftrightarrow [PPy^{0}] + SO_4^{2-} \qquad (1)$$

Furthermore, as mentioned before PPy can be reversibly switched between oxidized and reduced state, it can be used as a lithium-storage host. The charge storing mechanism in PPy as battery electrode materials can be explained as follows:

$$\text{At cathode: } [PPy^0] - e + PF_6^- \Leftrightarrow [PPy^+]PF_6^- \quad (2)$$

$$\text{At anode: } Li^+ + e^- \Leftrightarrow Li \quad (3)$$

It is further interesting to note that, due to nanoscale dimensions of PPy, extrinsic pseudo-capacitance is emerged which creates large fraction of Li^+ storage sites on the surface or near-surface region. Thus, PPy nanostructures can be used as electrode materials in both supercapacitors and Li-ion battery devices.

Conclusions

In summary, three different morphologies of polypyrrole: nanotubes, nanowires and urchins have been successfully prepared by a reactive-template assisted chemical polymerization route. The electrochemical performance of PPy nanostructures strongly depends on their morphologies. The hierarchical structures reported here exhibit outstanding advantages for energy storage. For supercapacitor applications, PPy-NFs deliver high specific capacitance of 604 and 285 F/g at high current densities of 1.81 and 18 A/g, respectively, with excellent cycling stability. Even after more than 1000 cycles at 9 A/g, a capacitance of 259 F/g at 9 A/g with 91 % retention was achieved for PPy-NFs. For LIBs application, PPy-NFs present a high reversible capacity of 70.2 mAh/g at 0.1 C with good cycling stability and rate capability. These excellent results highlight the advantage of fine-tuned nanostructures of PPy and show the way to design electrodes with higher energy storage performance together with low cost, ease of fabrication and high reproducibility.

Experimental details

Synthesis of MnO_2 nanorods

MnO_2 nanorods were prepared by a hydrothermal method. Briefly, 0.025 M of $KMnO_4$ was dissolved into 50 ml of deionized water in which 1.5 ml of concentrated HCl (37%) was added with stirring. The solution was transferred to a Teflon-lined stainless steel autoclave with a capacity of 100 ml. The autoclave was kept in an oven at a temperature of 140 °C for 16 hours. After reaction, the product was washed with deionized water and ethanol several times and dried in an oven overnight.

MnO_2 nanowires (Nw) and urchins have been synthesized by a simple co-precipitation method. Briefly, 0.1 M $MnSO_4$ and 0. 1 M $(NH_4)_2S_2O_8$ were used as sources of manganese and oxidizing agent, respectively. MnO_2 nanowires and urchins were prepared by using 0.05 M $(NH_4)_2SO_4$ and 0.05 M NH_4F, respectively. Both precursors were maintained at 353 K for 1 hr. The products were cleaned successively with water and ethanol and finally dried in an oven at 373 K overnight. The products obtained were further used as templates to prepare PPy nanostructures.

Synthesis of PPy nanostructures

Three different PPy nanostructures have been synthesized by using the corresponding three morphologies of MnO_2 as sacrificial templates. Typically, 100 mg of MnO_2 nanorods or urchins or nanowires were dispersed into 30 mL of deionized water with stirring for 15 min followed by bath sonication for 30 min in which 1 M HCl (37%) was added. Then 0.1 g of $K_2Cr_2O_7$ and 200 μl of pyrrole were added with stirring for 15 min followed by another 30 min of bath sonication. Later, the solution was stirred for 5 hours and maintained at room temperature for 24 hours. The product obtained was washed repeatedly with deionized water and ethanol and

then vacuum dried at 60 °C for 12 hours. Following the same strategy, three different nanostructures of PPy; nanotubes, urchins and nanofibers have been synthesized which are subsequently named PPy-NTs, PPy-Ur and PPy-NFs, respectively.

Electrode preparation and characterizations

To obtain a typical slurry, 85% of active material (PPy) was mixed with 10 % PVDF as binder and 5 % acetylene black. A fine mixture of active material, PVDF and acetylene black with NMP (solvent) was prepared. Finally the paste was applied on flexible carbon cloth which was further used as supercapacitors electrode. The mass loading of materials on the carbon cloth was obtained by measuring the weight difference before and after coating using a microbalance. The mass loaded (PPy) on the carbon cloth was between 1.1 to 1.3 mg/cm^2. Surface morphological analyses were carried out by scanning electron microscopy (FEI Quanta 650F Environmental SEM) and transmission electron microscopy (Tecnai G2 F20 S-TWIN HR(S) TEM, FEI). Powder X-ray diffraction study was performed using Panalytical X'pert Pro-MRD instrument (Cu K_α radiation and PIXel detector). The X-ray photoelectron spectra (XPS) analyses were obtained by X-ray photoelectron spectroscopy (XPS, SPECS Germany, PHOIBOS 150). N_2 adsorption/desorption was determined by Brunauer-Emmett-Teller (BET) measurements using Micromeritics instrument (Data Master V4.00Q, Serial#:2000/2400). Electrochemical characterization of PPy nanostructures was carried out in 3-electrode configuration with Biologic VMP3 potentiostat. Electrochemical properties were investigated by assembling three-electrode cells comprising a working electrode (area of 0.8 cm^2 PPy coated on carbon cloth), counter electrode (platinum wire) and reference electrode (sat. Ag/AgCl) in 1 M H_2SO_4 electrolyte.

Acknowledgements

Authors appreciate the award to DPD with the support of the Secretary for Universities and Research of the Ministry of Economy and Knowledge of the Government of Catalonia and the Co-fund programme of the Marie Curie Actions of the 7th R&D Framework Programme of the European Union" and the award of Humboldt Fellowship of the Alexander von Humboldt Foundation (AvH), Germany. ICN2 acknowledges support of the Spanish MINECO through the Severo Ochoa Centers of Excellence Program under Grant SEV-2013-0295.

References

[1] Lou, X. W.; Archer, L. A.; Yang, Z. C.; Hollow Micro-/Nanostructures: Synthesis and Application *Adv. Mater.*, **2008**, *20*, 3987-4019.

[2] Lokhande, C. D.; Dubal, D. P.; Joo, O. S.; Metal Oxide Thin Film based Supercapacitors *Curr. Appl. Phys.* **2011**, *11*, 255-270

[3] Dubal, D. P.; Gomez-Romero, P.; Sankapal, B. R.; Holze, R.; Nickel Cobaltite as an Emerging Material for Supercapacitors: An Overview *Nano Energy*, **2015**, *11*, 377-399

[4] Dubal, D. P.; Ayyad, O.; Ruiz, V.; Gomez-Romero, P.; Hybrid Energy Storage: The Merging of Battery and Supercapacitor Chemistries *Chem. Soc. Rev.*, **2015**, *44*, 1777-1790

[5] Miller, J. R.; Simon, P.; Electrochemical Capacitors for Energy Management *Science*, **2008**, *321*, 651-652

[6] Tarascon, J. M.; Armand, M.; Issues and Challenges Facing Rechargeable Lithium Batteries *Nature*, **2001**, *414*, 359-367

[7] Zhang, Y.; Li, L.; Su, H.; Huang, W.; Dong, X.; Binary Metal Oxide: Advanced Energy Storage Materials in Supercapacitors *J. Mater. Chem. A*, **2015**, *3*, 43-59

[8] Simon, P.; Gogotsi, Y.; Materials for Electrochemical Capacitors *Nat. Mater.*, **2008**, *7*, 845-854

[9] Dubal, D. P.; Kim, J. G.; Kim, Y.; Holze, R.; Lokhande, C. D.; Kim, W. B.; Supercapacitors Based on Flexible Substrates: An Overview *Energy Technol.* **2014**, *2*, 325-341

[10] Kim, M. G.; Cho, J.; Reversible and High-Capacity Nanostructured Electrode Materials for Li-Ion Batteries *Adv. Funct. Mater.*, **2009**, *19*, 1497-1514

[11] Chen, Y.; Qu, B.; Hu, L.; Xu, Z.; Li, Q.; Wang, T.; High-Performance Supercapacitor and Lithium-ion Battery based on 3D Hierarchical NH_4F-induced Nickel Cobaltate Nanosheet-Nanowire Cluster Arrays as Self-supported Electrodes *Nanoscale*, **2013**, *5*, 9812-9820

[12] Dubal, D. P.; Holze, R.; High Capacity Rechargeable Battery Electrode based on Mesoporous Stacked Mn_3O_4 Nanosheets *RSC Adv*., **2012**, *2*, 12096-12100

[13] Armand, M.; Tarascon, J. M.; Building Better Batteries *Nature*, **2008**, *451*, 652-657

[14] Bruce, P. G.; Scrosati, B.; Tarascon, J. M.; Nanomaterials for Rechargeable Lithium Batteries *Angew. Chem., Int. Ed.*, **2008**, *47*, 2930-2946

[15] Goodenough, J. B.; Kim, Y.; Challenges for Rechargeable Li Batteries *Chem. Mater.*, **2010**, *22*, 587-603

[16] Tran, H. D.; Li, D.; Kaner, R. B.; One-Dimensional Conducting Polymer Nanostructures: Bulk Synthesis and Applications *Adv. Mater*., **2009**, *21*, 1487-1499

[17] Gómez-Romero, P.; Chojak, M.; Cuentas-Gallegos, K.; Asensio, J. A.; Kulesza, P. J.; Casañ-Pastor, N.; Lira-Cantú, M.; Hybrid Organic-Inorganic Nanocomposite Materials for Application in Solid State Electrochemical Supercapacitors *Electrochem. Commun.*, **2003**, *5*, 149-153

[18] Cho, S. I.; Lee, S. B.; Fast Electrochemistry of Conductive Polymer Nanotubes: Synthesis, Mechanism, and Application *Acc. Chem. Res.*, **2008**, *41*, 699-707

[19] Aleshin, A. N.; Polymer Nanofibers and Nanotubes: Charge Transport and Device Applications *Adv. Mater.*, **2006**, *18*, 17-27

[20] Ramya, R.; Sivasubramanian, R.; Sangaranarayanan, M. V.; Conducting Polymers-based Electrochemical Supercapacitors-Progress and Prospects *Electrochim. Acta,* **2013**, *101*, 109-129

[21] Yan, F.; Xue, G.; Wan, F.; A Flexible Giant Magnetoresistance Sensor Prepared Completely by Electrochemical Synthesis *J. Mater. Chem.*, **2002**, *12*, 2606-2608

[22] Li, X.; Zhitomirsky, I.; Electrodeposition of Polypyrrole-Carbon Nanotube Composites for Electrochemical Supercapacitors *J. Power Sources*, **2013**, *221*, 49-56

[23] Holze, R.; Wu, Y. P.; Intrinsically Conducting Polymers in Electrochemical Energy Technology: Trends and Progress *Electrochim. Acta*, **2014**, *122*, 93-107

[24] Jang, J.; Yoon, H.; Formation Mechanism of Conducting Polypyrrole Nanotubes in Reverse Micelle Systems *Langmuir*, **2005**, *21*, 11484-11489

[25] Yang, X.; Zhu, Z.; Dai, T.; Lu, Y.; Electrochemical Synthesis of Functional Polypyrrole Nanotubes via a Self-Assembly Process *Polymer*, **2007**, *48*, 4021-4027

[26] Dai, T.; Yang, X.; Lu, Y.; Controlled Growth of Polypyrrole Nanotubule/wire in the Presence of a Cationic Surfactant *Nanotechnol.*, **2006**, *17*, 3028-3034

[27] Zhang, J.; Liu, X.; Zhang, L.; Cao, B.; Wu, S,; Reactive Template Synthesis of Polypyrrole Nanotubes for Fabricating Metal/Conducting Polymer Nanocomposites *Macromol. Rapid Commun.*, **2013**, *34*, 528-532

[28] Wang, J. G.; Wei, B.; Kang, F.; Facile Synthesis of Hierarchical Conducting Polypyrrole Nanostructures via a Reactive Template of MnO_2 and Their Application in Supercapacitors *RSC Adv.*, **2014**, *4*, 199-202

[29] Noh, K. A.; Kim, D. W.; Jin, C. S.; Shin, K. H.; Kim, J. H.; Jo, J. M.; Synthesis and Pseudo-capacitance of Chemically-Prepared Polypyrrole Powder *J. Power Sources*, **2003**, *124*, 593-595

[30] Wang, X.; Li, Y.; Selected-control Hydrothermal Synthesis of Alpha- and Beta-MnO_2 Single Crystal Nanowires *J. Am. Chem. Soc.*, **2002**, *124*, 2880-2881

[31] Luo, Y. L.; Fan, L. H.; Xu, F.; Chen, Y. S.; Zhang, C. H.; Wei, Q. B.; Synthesis and Characterization of Fe_3O_4/PPy/P(MAA-co-AAm) Trilayered Composite Microspheres with Electric, Magnetic and pH Response Characteristics *Mater. Chem. Phys.*, **2010**, *120*, 590-597

[32] Singh, A.; Salmi, Z.; Joshi, N.; Jha, P.; Kumar, A.; Lecoq, H.; Lau, S.; Chehimi, M. M.; Aswal, D. K.; Gupta, S. K.; Photo-induced Synthesis of Polypyrrole-Silver Nanocomposite Films on *N*-(3-trimethoxysilylpropyl)pyrrole-modified Biaxially Oriented Polyethylene Terephthalate Flexible Substrates *RSC Adv.*, **2013**, *3*, 5506-5523

[33] Lim, S. P.; Pandikumar, A.; Lim, Y. S.; Huang, N. M.; Lim, H. N.; In-situ Electrochemically Deposited Polypyrrole Nanoparticles Incorporated Reduced Graphene Oxide as an Efficient Counter Electrode for Platinum-free Dye-sensitized Solar Cells *Sci. Rep.*, **2014**, *4*, 5305

[34] Sreedhar, B.; Sairam, M.; Chattopadhyay, D. K.; Mitra, P. P.; Rao, D. V. M.; Thermal and XPS Studies on Polyaniline Salts Prepared by Inverted Emulsion Polymerization *J. Appl. Polym. Sci.*, **2006**, *101*, 499-508

[35] Li, Y.; Neoh, K. G.; Cen, L.; Kang, E. T.; Porous and Electrically Conductive Polypyrrole-Poly(vinyl alcohol) Composite and Its Applications as a Biomaterial *Langmuir*, **2005**, *21*, 10702-10709

[36] Sharma, M.; Waterhouse, G. I. N.; Loader, S. W. C.; Garg, S.; Svirskis, D.; High Surface Area Polypyrrole Scaffolds for Tunable Drug Delivery *International J. Pharm.*, **2013**, *443*, 163-168

[37] Dubal, D. P.; Lee, S. H.; Kim, J. G.; Kim, W. B.; Lokhande, C. D.; Porous Polypyrrole Clusters Prepared by Electropolymerization for a High Performance Supercapacitor *J. Mater. Chem.*, **2012**, *22*, 3044-3052

[38] Shinde, S. S.; Gund, G. S.; Dubal, D. P.; Jambure, S. B.; Lokhande, C. D.; Morphological Modulation of Polypyrrole Thin Films Through Oxidizing Agents and Their Concurrent Effect on Supercapacitor Performance *Electrochim. Acta*, **2014**, 119, 1-10

[39] Snook, G. A.; Kao, P.; Best, A. S.; Conducting-polymer-based Supercapacitor Devices and Electrodes *J. Power Sources*, **2011**, *196*, 1-12

[40] Wang, J. G.; Wei, B.; Kang, F.; Facile Synthesis of Hierarchical Conducting Polypyrrole Nanostructures *via* a Reactive Template of MnO_2 and Their Application in Supercapacitors *RSC Adv.*, **2014**, *4*, 199-202

[41] Liu, J. H.; An, J. W.; Ma, Y. X.; Li, M. L.; Ma, R. B.; Yu, M.; Li, S. M.; Electrochemical Properties Comparison of the Polypyrrole Nanotube and Polyaniline Nanofiber Applied in Supercapacitor *Eur. Phys. J.: Appl. Phys.*, **2012**, *57*, 30702

[42] Mi, H.; Zhang, X.; Ye, X.; Yang, S.; Preparation and Enhanced Capacitance of Core-Shell Polypyrrole/Polyaniline Composite Electrode for Supercapacitors *J. Power Sources*, **2008**, *176*, 403-409

[43] Wu, Q. F.; He, K. X.; Mi, H. Y.; Zhang, X. G.; Electrochemical Capacitance of Polypyrrole Nanowire Prepared by Using Cetyltrimethylammonium Bromide (CTAB) as Soft Template *Mater. Chem. Phys.*, **2007**, *101*, 367-371

[44] Li, J.; Cui, L.; Zhang, X.; Preparation and Electrochemistry of One-Dimensional Nanostructured MnO_2/PPy Composite for Electrochemical Capacitor *Appl. Surf. Sci.*, **2010**, *256*, 4339-4343

[45] Fan, L. Z.; Maier, J.; High-performance polypyrrole electrode materials for redox supercapacitors *Electrochem. Commun.* **2006**, *8*, 937-940

[46] Shi, Y.; Pan, L.; Liu, B.; Wang, Y.; Cui, Y.; Bao, Z.; Yu, G.; Nanostructured conductive polypyrrole hydrogels as high-performance, flexible supercapacitor electrodes *J. Mater. Chem. A*, **2014**, *2*, 6086-6091

[47] Oliveira, H. P.; Sydlik, S. A.; Swager, T. M.; Supercapacitors from Free-Standing Polypyrrole/Graphene Nanocomposites *J. Phys. Chem. C*, **2013**, *117*, 10270-10276

[48] Zhang, F.; Xiao, F.; Dong, Z. H., Shi, W.; Synthesis of polypyrrole wrapped graphene hydrogels composites as supercapacitor electrodes *Electrochim. Acta.*, **2013**, *114*, 125-132

[49] Park, K. S.; Schougaard, S. B.; Goodenough, J. B.; Conducting-Polymer/Iron-Redox-Couple Composite Cathodes for Lithium Secondary Batteries *Adv. Mater.*, **2007**, *19*, 848-851

[50] Qie, L.; Yuan, L. X.; Zhang, W. X.; Chen, W. M.; Huang, Y. H.; Revisit of Polypyrrole as Cathode Material for Lithium-Ion Battery *J. Electrochem. Soc.*, **2012**, *159*, A1624

[51] Simon, P.; Gogotsi, Y.; Dunn, B.; Where Do Batteries End and Supercapacitors Begin? *Science*, **2014**, *343*, 1210-1211

[52] Brousse, T.; Belanger, D.; Long, J. W.; To Be or Not To Be Pseudocapacitive? *J. Electrochem. Soc.*, **2015**, *162*, A5185-A5189

Figure captions

Fig. 1 SEM images of three different nanostructures of MnO_2 (a) nanorods (b) nanowires and (c) urchins with corresponding morphologies of PPy (d) nanotubes, (e) nanofibers and (f) urchins, respectively.

Fig. 2 Schematic illustration of steps involved in growth of PPy nanostructures by the tunable morphology of MnO_2 as reactive templates

Fig. 3 TEM images of PPy nanostructures (a) nanotubes, PPy-NTs (b) nanofibers, PPy-NFs and (c) urchins, PPy-Urs with corresponding SAED pattern of PPy-Urs (d).

Fig. 4 (a) XRD patterns (b) Full XPS spectra of three different nanostructures of PPy: PPy-NTs, PPy-NFs and PPy-Urs, respectively.

Fig. 5 (a) Nitrogen adsorption/desorption isotherm of PPy-NTs, PPy-NFs and PPy-Urs samples, respectively (b) corresponding pore size distribution plots.

Fig. 6 (a-c) Cyclic voltammetry curves of PPy-NTs, PPy-NFs and PPy-Urs electrodes at different scanning rates, respectively, (d-f) Galvanostatic charge/discharge (CD) curves of PPy-NTs, PPy-NFs and PPy-Urs electrodes at different current densities.

Fig. 7 (a) Variation of specific capacitance of PPy-NTs, PPy-NFs and PPy-Urs electrodes with current density (b) Plots areal capacitance versus current density for PPy-NTs, PPy-NFs and

PPy-Urs, (c) Variation of volumetric capacitance of PPy-NTs, PPy-NFs and PPy-Urs electrodes with current density, (d) variation of specific capacitance of PPy-NTs, PPy-NFs and PPy-Urs electrodes with number of cycles at 9 A/g current density.

Fig. 8 (a) Cell voltage as a function of the capacity for the 5th cycle at 0.10 (b) discharge capacity at different C-rate (c) discharge capacity of the last 100 cycles at 1 C (d) Nyquist plot before and after cycling PPy-NTs, PPy-NFs and PPy-Urs electrodes

Figure(s)

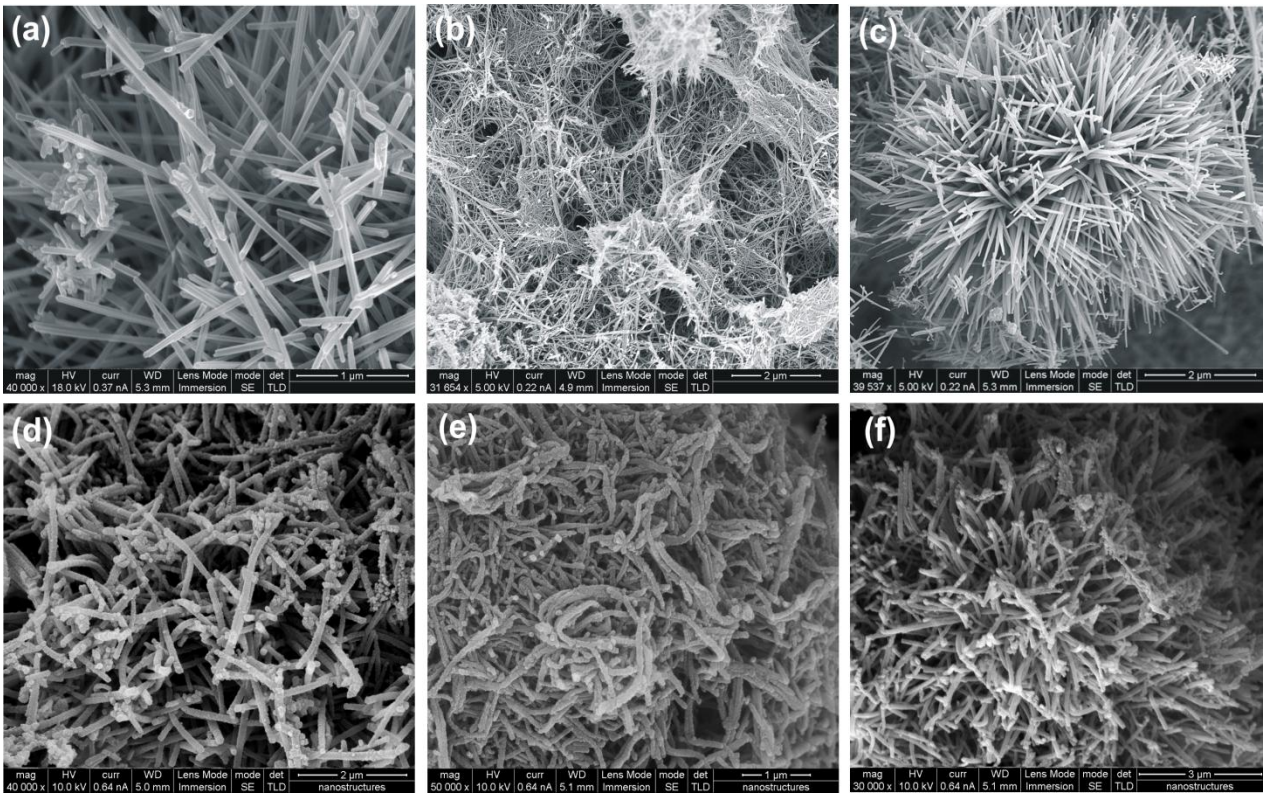

Fig. 1

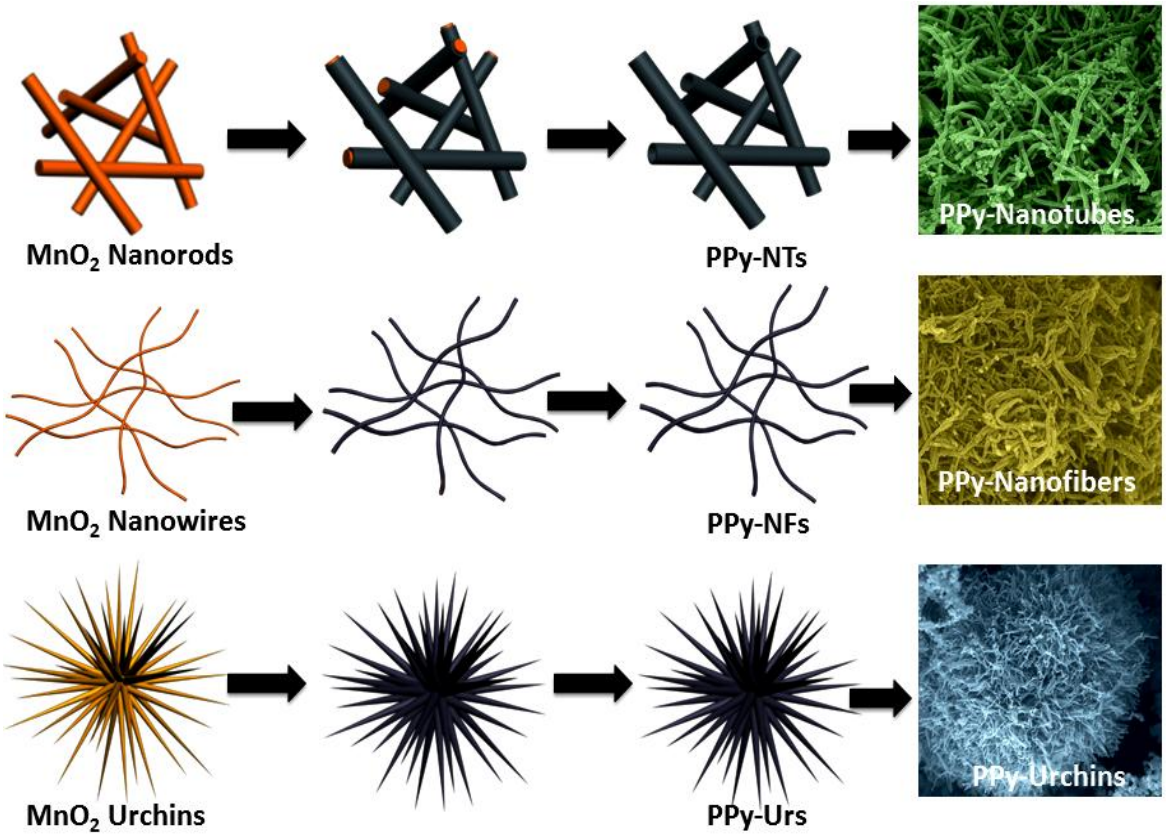
MnO2 Nanorods
PPy-NTs
PPy-Nanotubes
MnO2 Nanowires
PPy-NFs
PPy-Nanofibers
MnO2 Urchins
PPy-Urs
PPy-Urchins

Fig. 2

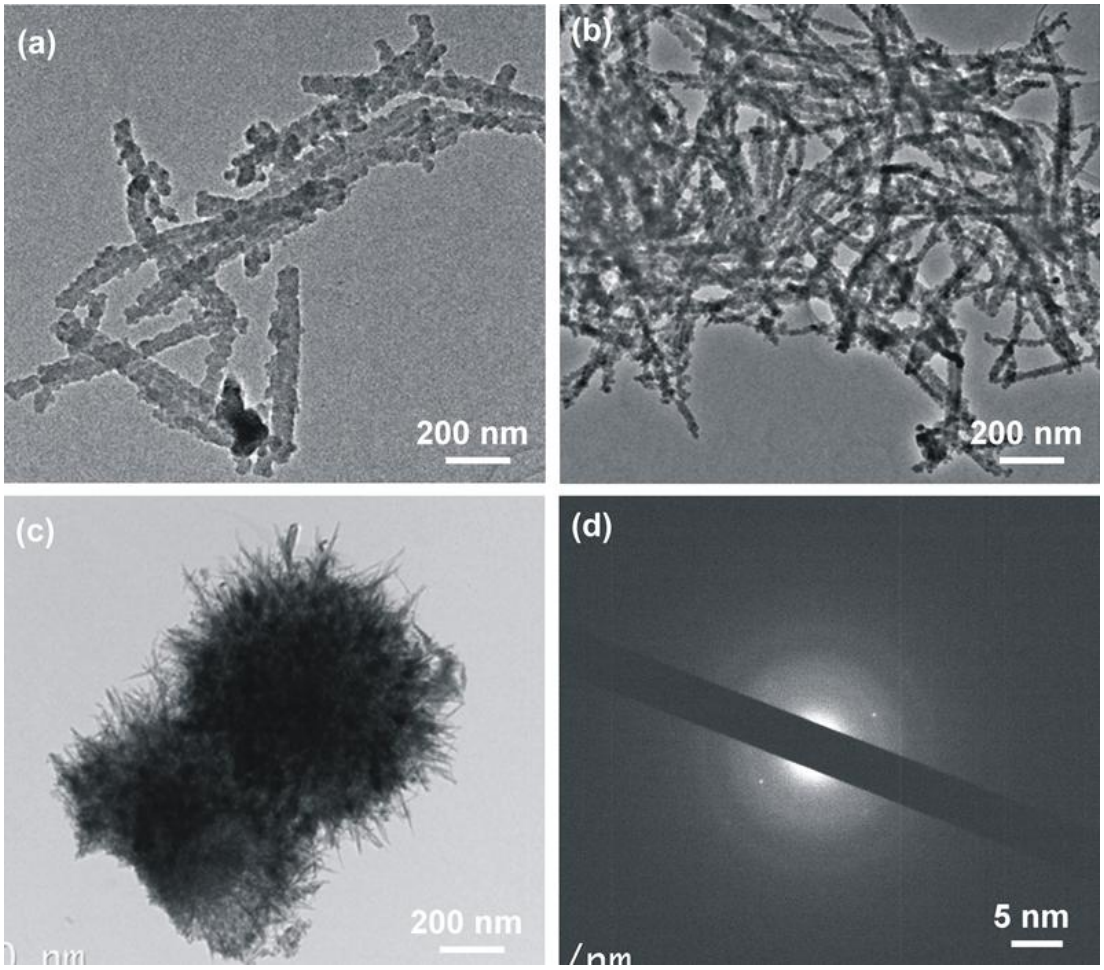

Fig. 3

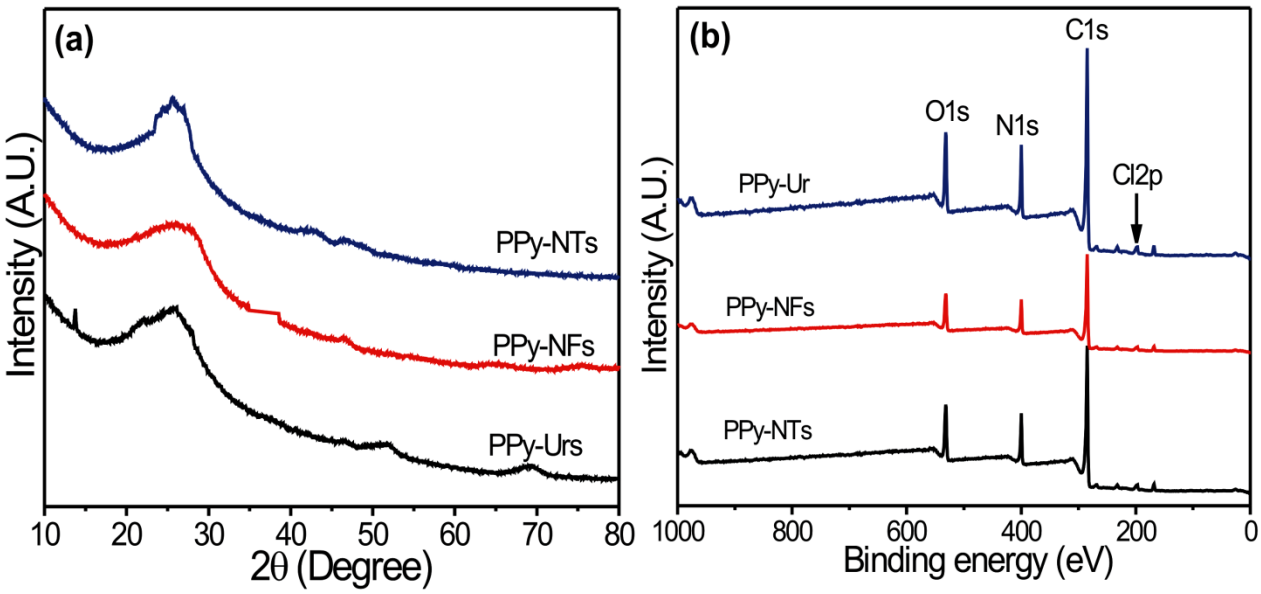
(a)
Intensity (A.U.)
PPy-NTs
PPy-NFs
PPy-Urs
10
20
30
40
50
60
70
80
2θ (Degree)
(b)
C1s
O1s
N1s
Cl2p
PPy-Ur
PPy-NFs
PPy-NTs
Intensity (A.U.)
1000
800
600
400
200
0
Binding energy (eV)

Fig. 4

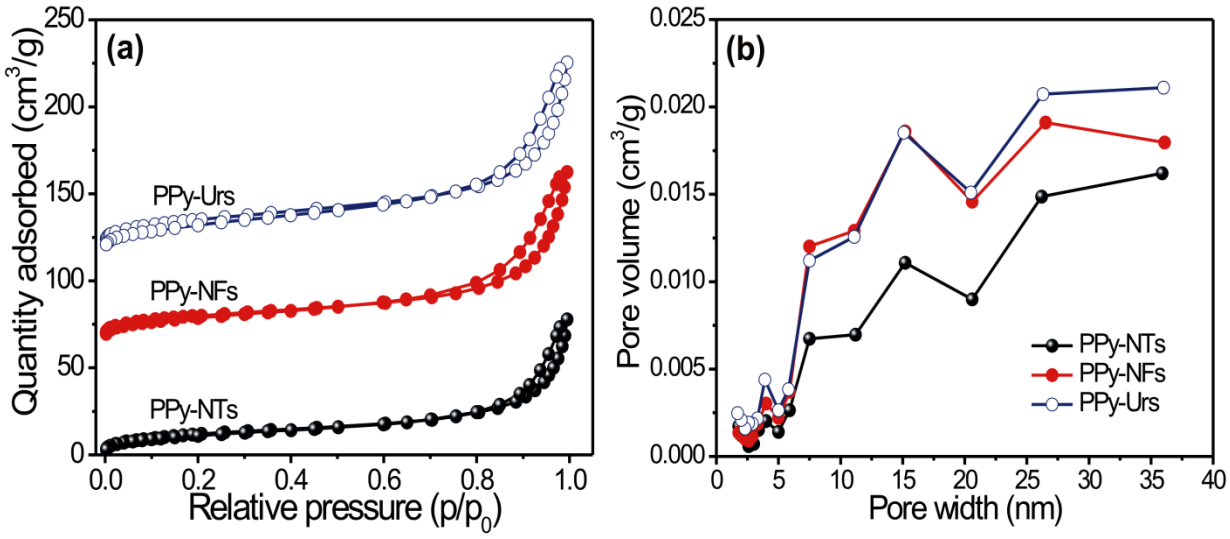
(a)
Quantity adsorbed (cm3/g)
Relative pressure (p/p0)
PPy-Urs
PPy-NFs
PPy-NTs
(b)
Pore volume (cm3/g)
Pore width (nm)
PPy-NTs
PPy-NFs
PPy-Urs

Fig. 5

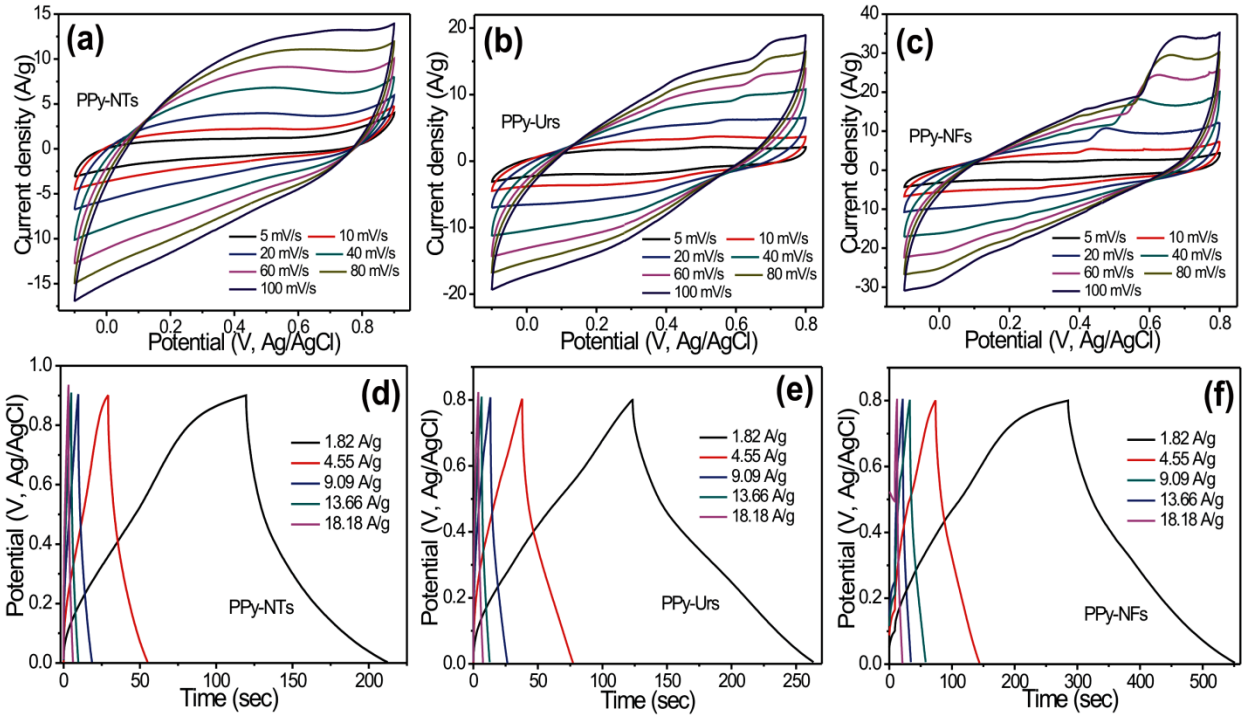
(a)
PPy-NTs
Current density (A/g)
Potential (V, Ag/AgCl)
5 mV/s
10 mV/s
20 mV/s
40 mV/s
60 mV/s
80 mV/s
100 mV/s
(b)
PPy-Urs
(c)
PPy-NFs
(d)
Potential (V, Ag/AgCl)
Time (sec)
1.82 A/g
4.55 A/g
9.09 A/g
13.66 A/g
18.18 A/g
(e)
(f)

Fig. 6

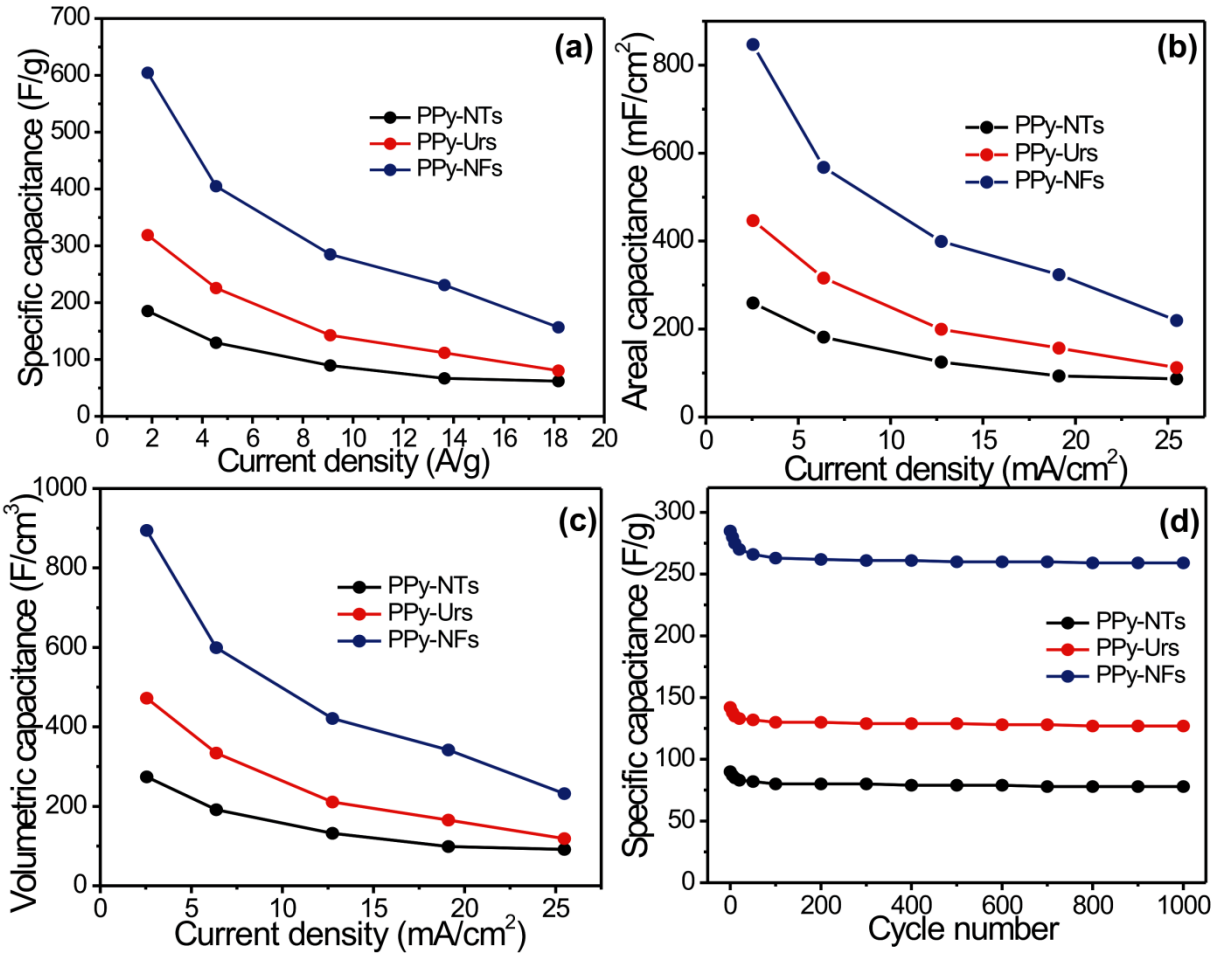
(a)
Specific capacitance (F/g)
Current density (A/g)
PPy-NTs
PPy-Urs
PPy-NFs
(b)
Areal capacitance (mF/cm^2)
Current density (mA/cm^2)
PPy-NTs
PPy-Urs
PPy-NFs
(c)
Volumetric capacitance (F/cm^3)
Current density (mA/cm^2)
PPy-NTs
PPy-Urs
PPy-NFs
(d)
Specific capacitance (F/g)
Cycle number
PPy-NTs
PPy-Urs
PPy-NFs

Fig. 7

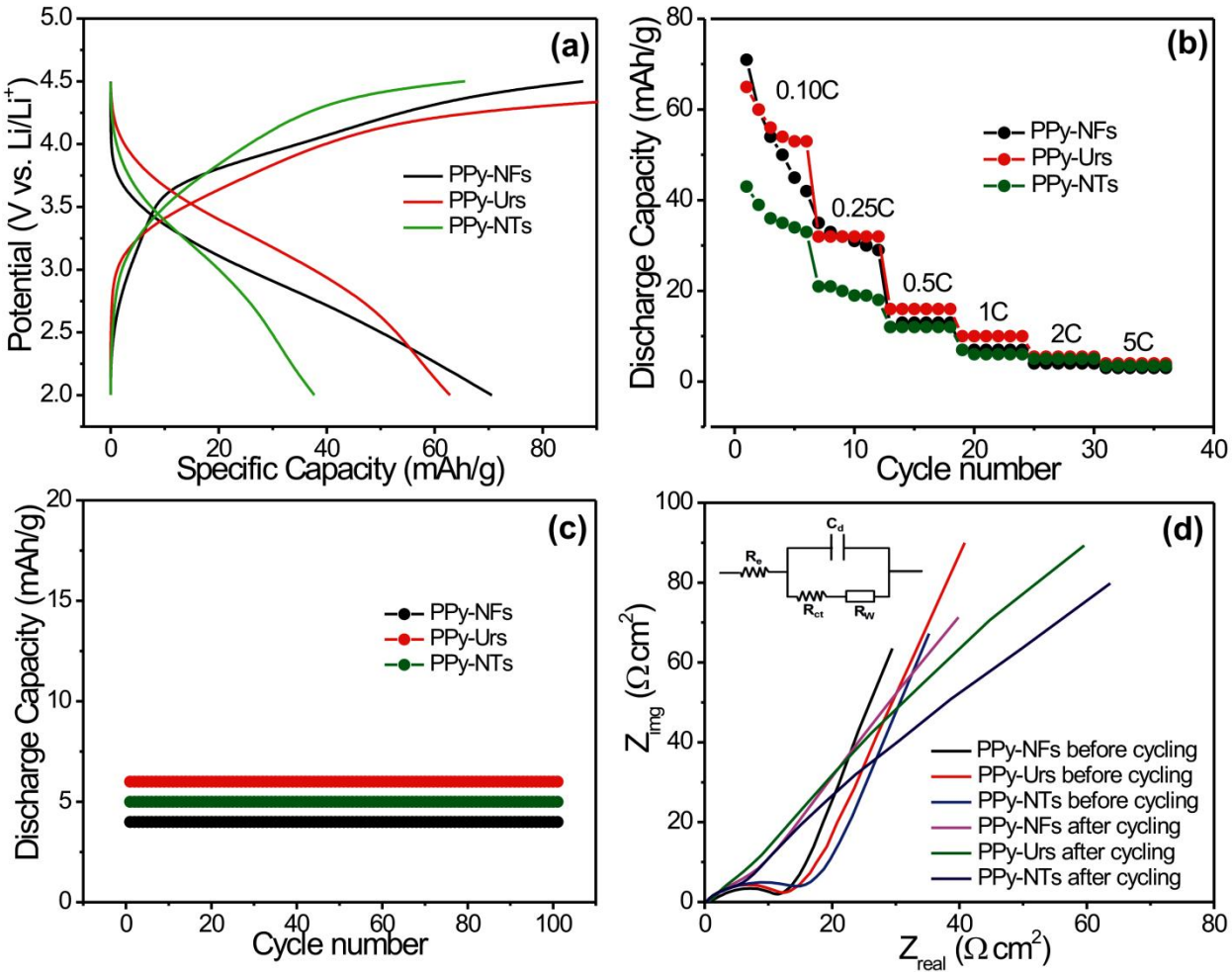
(a)
Potential (V vs. Li/Li+)
Specific Capacity (mAh/g)
PPy-NFs
PPy-Urs
PPy-NTs
(b)
Discharge Capacity (mAh/g)
Cycle number
0.10C
0.25C
0.5C
1C
2C
5C
PPy-NFs
PPy-Urs
PPy-NTs
(c)
Discharge Capacity (mAh/g)
Cycle number
PPy-NFs
PPy-Urs
PPy-NTs
(d)
Zimg (Ω cm2)
Zreal (Ω cm2)
Cd
Rs
Rct
RW
PPy-NFs before cycling
PPy-Urs before cycling
PPy-NTs before cycling
PPy-NFs after cycling
PPy-Urs after cycling
PPy-NTs after cycling

Fig. 8

Graphical Abstract

SEM images of three different PPy nanostructures synthesized by using three different nanostructures of MnO_2 as sacrificial templates.